FedProf: Selective Federated Learning with Representation Profiling

Wentai Wu, Ligang He, Weiwei Lin, and Rui Mao

Abstract

Federated Learning (FL) has shown great potential as a privacy-preserving solution to learning from decentralized data that are only accessible to end devices (i.e., clients). In many scenarios however, a large proportion of the clients are probably in possession of low-quality data that are biased, noisy or even irrelevant. As a result, they could significantly slow down the convergence of the global model we aim to build and also compromise its quality. In light of this, we propose FEDPROF, a novel algorithm for optimizing FL under such circumstances without breaching data privacy. The key of our approach is a data representation profiling and matching scheme that uses the global model to dynamically profile data representations and allows for low-cost, lightweight representation matching. Based on the scheme we adaptively score each client and adjust its participation probability so as to mitigate the impact of low-value clients on the training process. We have conducted extensive experiments on public datasets using various FL settings. The results show that FEDPROF effectively reduces the number of communication rounds and overall time (up to 4.5x speedup) for the global model to converge and provides accuracy gain.

I. INTRODUCTION

With the advances in Artificial Intelligence (AI), we are seeing a rapid growth in the number of AI-driven applications as well as the volume of data required to train them. However, a large proportion of data used for machine learning are often generated outside the data centers by distributed resources such as mobile phones and IoT (Internet of Things) devices. It is predicted that the data generated by IoT devices will account for 75% in 2025 [1]. Under this circumstance, it will be very costly to gather all the data for centralized training. More importantly, moving the data out of their local devices (e.g., mobile phones) is now restricted by law in many countries, such as the General Data Protection Regulation (GDPR)¹ enforced in EU.

We face three main difficulties to learn from decentralized data: i) massive scale of end devices; ii) limited communication bandwidth at the network edge; and iii) uncertain data distribution and data quality. As an promising solution, Federated Learning (FL) [2] is a framework for efficient distributed machine learning with privacy protection (i.e., no data exchange). A typical process of FL is organized in rounds where the devices (clients) download the global model from the server, perform local training on their data and then upload their updated local models to the server for aggregation. Compared to traditional distributed learning methods, FL is naturally more communication-efficient at scale [3][4]. Nonetheless, several issues stand out.

A. Motivation

1) FL is susceptible to biased and low-quality local data. Only a fraction of clients are selected for a round of FL (involving too many clients leads to diminishing gains [35]). The standard FL algorithm [2] selects clients randomly, which implies that every client (and its local data) is considered equally important. This makes the training process susceptible to local data with strong heterogeneity and of low quality (e.g., usergenerated texts [7] and noisy photos). In some scenarios, local data may contain irrelevant or even adversarial samples [8][9] from malicious clients [12][9][13]. Traditional solutions such as data augmentation [14] and re-sampling [10] prove useful for centralised training but applying them to local datasets may introduce extra noise [11] and increase the risk of information leakage [15]. Another naive solution is to directly exclude those low-value clients with low-quality data, which, however, is often impractical because i) the quality of

W. Wu, L. He (corresponding author, ligang.he@warwick.ac.uk) are with the Department of Computer Science, University of Warwick. W. Lin is with the School of Computer Science and Engineering, South China University of Technology. Rui Mao is with the College of Computer Science and Software Engineering, Shenzhen University, China

¹https://gdpr.eu/what-is-gdpr/

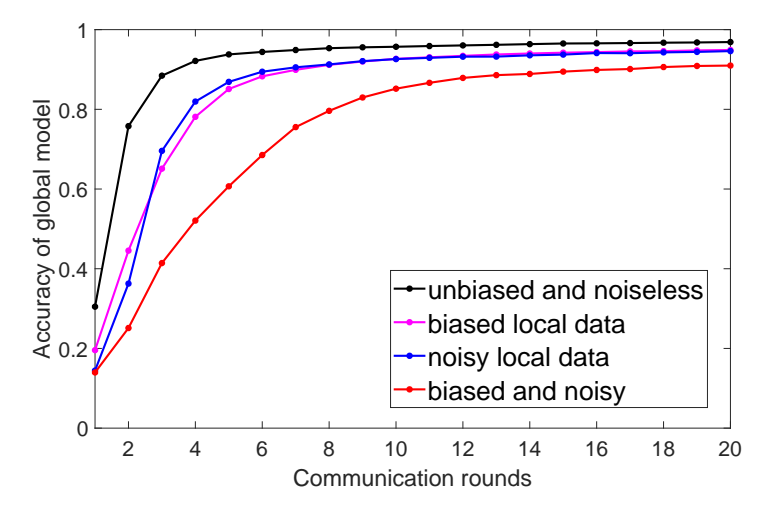


Fig. 1: (Preliminary experiment) The global model's convergence under different data conditions. We ran the FL process with 100 clients to learn a CNN model on the MNIST dataset, which is partitioned and allocated to clients in four different ways where the data are 1) *original* (black line): noiseless and evenly distributed across the clients, 2) *biased* (magenta line): locally class-imbalanced, 3) *noisy* (blue line): blended with noise, and 4) *biased and noisy* (red line). The noise (if applied) covers 65% of the clients; the dominant class accounts for >50% of the samples for biased local data.

the data depends on the learning task and is difficult to gauge; ii) some noisy or biased data could be useful to the training at early stages [16]; and iii) sometimes low-quality data are very common across the clients.

In Fig. 1 we demonstrate the impact of involving "low-value" clients by running FL over 100 clients to learn a CNN model on MNIST using the standard FEDAVG algorithm. From the traces we can see that training over clients with problematic or strongly biased data can compromise the efficiency and efficacy of FL, resulting in an inferior global model that takes more rounds to converge.

2) Learned representations can reflect data distribution and quality. Representation learning is vital to the performance of deep models because learned representations can capture the intrinsic structure of data and provide useful information for the downstream machine learning tasks [17]. The value of representations also lies in the fact that they characterize the domain and learning task using the model as a medium [18][19]. The similarity of representations are also used for refining the model update rules in FL [20][21]. Inspired by these studies, we propose to use representations as the "lens" to reflect the training value of local data.

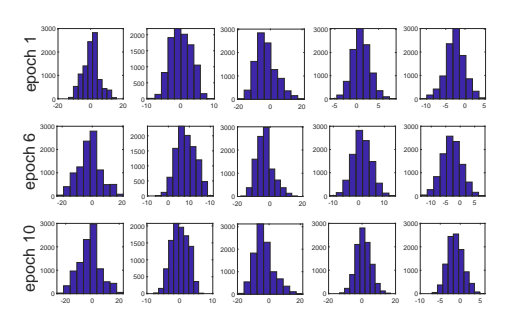
Our study is also motivated by a key observation that representations from neural networks tend to have Gaussian patterns. As a demonstration we trained two different models (LeNet-5 and ResNet-18) on two different datasets (MNIST and CIFAR-100) separately. Fig. 2a shows the neuron-wise distribution of representations extracted from the first dense layer (FC-1) of LeNet-5. Fig. 2b shows the distribution of fused representations (in a channel-wise manner) extracted from a plain convolution layer and a residual block of ResNet-18.

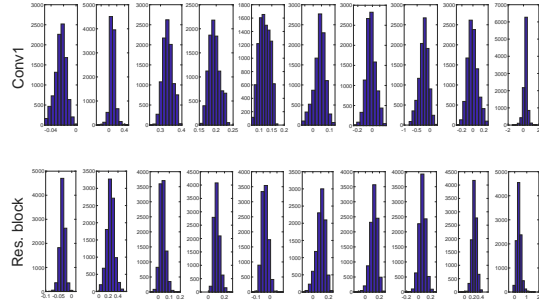
These observations motivate us to study the distributional property of data representations and use it as a means to differentiate clients' value.

B. Contributions

Our contributions are summarized as the following:

• We first provide theoretical proof for the observation that data representations from neural networks tend to follow Gaussian distribution, based on which we propose a representation profiling and matching scheme for fast, low-cost comparison between different representation profiles.





- (a) Representations from FC-1 of a LeNet-5 model (b) Fused representations from a standard convolution after being trained for 1, 6 and 10 epochs on MNIST. layer (1st row) and a residual block (2nd row) of a ResNet-18 model trained for 100 epochs on CIFAR-100.

Fig. 2: (Preliminary experiment) Demonstration of learned representations from a distributional perspective. The representations are generated by forward propagation in model evaluation. Each box corresponds to a randomly sampled element in the whole layer-wise representation.

- We present a novel FL algorithm FEDPROF that adaptively adjusts clients' participation probability based on representation profile dissimilarity.
- Results of extensive experiments show that FEDPROF reduces the number of communication rounds by up to 77%, shortens the overall training time (up to 4.5x speedup) while increasing the accuracy of the global model by up to 2.5%.

II. RELATED WORK

Different from traditional distributed training methods (e.g., [22][23][24]), Federated Learning assumes strict constraints of data locality and limited communication capacity [3]. Much effort has been made in optimizing FL and covers a variety of perspectives including communication [3][26][28], update rules [36][6][34][29], flexible aggregation [4][27] and personalization [32][30][31].

The control of device participation is imperative in cross-device FL scenarios [5][25] where the quality of local data is uncontrollable and the clients show varied value for the training task [49]. To this end, the selection of clients is pivotal to the convergence of FL over heterogeneous data and devices [37][38][39][40]. Non-uniform client selection is widely adopted in existing studies [36][50][51][35][41][46] and has been theoretically proven with convergence guarantees [41][35]. Many approaches sample clients based on their performance [37][45] or aim to jointly optimize the model accuracy and training time [42][43][44]. A popular strategy is to use loss as the information to guide client selection [50][47][48]. For example, AFL [50] prioritizes the clients with high loss feedback on local data, but it is potentially susceptible to noisy and unexpected data that yield illusive loss values. Data representations are useful for knowledge exchange in FL [20][21]. Inspired by these studies, our work seeks to optimize client selection using representations as the key information.

III. DATA REPRESENTATION PROFILING AND MATCHING

In this paper, we consider a typical cross-device FL setting [5], in which multiple end devices collaboratively perform local training on their own datasets D_i , i = 1, 2, ..., n. The server owns a validation dataset D^* for model evaluation. Every dataset is only accessible by its owner.

Considering the distributional pattern of data representations (Fig. 2) and the role of the global model in FL, we propose to profile the representations of local data using the global model. In this section, we first provide theoretical proof to support our observation that representations from neural network models tend to follow Gaussian distribution. Then we present a novel scheme to profile data representations and define profile dissimilarity for fast and secure representation comparison.

A. Gaussian Distribution of Representations

We first make the following definition to facilitate our analysis.

Definition 1 (The Lyapunov's condition). A set of random variables $\{Z_1, Z_2, \dots, Z_v\}$ satisfies the Lyapunov's condition if there exists a δ such that

$$\lim_{v \to \infty} \frac{1}{s^{2+\delta}} \sum_{k=1}^{v} E\left[|Z_k - \mu_k|^{2+\delta} \right] = 0, \tag{1}$$

where
$$\mu_k = E[Z_k]$$
, $\sigma_k^2 = E[(Z_k - \mu_k)^2]$ and $s = \sqrt{\sum_{k=1}^v \sigma_k^2}$.

The Lyapunov's condition can be intuitively explained as a limit on the overall variation (with $|Z_k - \mu_k|^{2+\delta}$ being the $(2+\delta)$ -th moment of Z_k) of a set of random variables.

Now we present Proposition 1 and Proposition 2.

Proposition 1. The representations from linear operators (e.g., a pre-activation dense layer or a plain convolutional layer) in a neural network tend to follow the Gaussian distribution if the layer's weighted inputs satisfy the Lyapunov's condition.

Proposition 2. The fused representations² from non-linear operators (e.g., a hidden layer of LSTM or a residual block of ResNet) in a neural network tend to follow the Gaussian distribution if the layer's output elements satisfy the Lyapunov's condition.

The proofs of Propositions 1 and 2 are provided in Appendices A-A and A-B, respectively. In practice, the Lyapunov's condition is typically met when the model is properly initialized and batch normalization is applied. Next, we discuss the proposed representation profiling and matching scheme.

B. Distributional Profiling and Matching

Based on the Gaussian pattern of representations, we compress the data representations statistically into a compact form called *representation profiles*. The profile produced by the global model w on a dataset D, denoted by RP(w,D), has the following format:

$$RP(w, D) = \{ \mathcal{N}(\mu_i, \sigma_i^2) \}_{i=1}^q,$$
 (2)

where q is the profile length determined by the dimensionality of the representations. For example, q is equal to the number of kernels for channel-wise fused representations from a convolutional layer. The tuple (μ_i, σ_i^2) contains the mean and the variance of the i-th representation element.

Local representation profiles are generated by clients and sent to the server for comparison (the cost of transmission is negligible considering each profile is only $q \times 8$ bytes). Let RP_k denote the local profile from client k, and RP^* denote the baseline profile (generated in model evaluation) on the server. The dissimilarity between RP_k and RP^* , denoted by $div(RP_k, RP^*)$, is defined as:

$$div(RP_k, RP^*) = \frac{1}{q} \sum_{i=1}^{q} KL(\mathcal{N}_i^{(k)}||\mathcal{N}_i^*), \tag{3}$$

where $KL(\cdot)$ denotes the Kullback–Leibler (KL) divergence. An advantage of our profiling scheme is that a much simplified KL divergence formula can be adopted because of the Gaussian distribution property (see Appendix B, ref. [53] for details), which yields:

$$KL(\mathcal{N}_i^{(k)}||\mathcal{N}_i^*) = \log \frac{\sigma_i^*}{\sigma_i^{(k)}} + \frac{(\sigma_i^{(k)})^2 + (\mu_i^{(k)} - \mu_i^*)^2}{2(\sigma_i^*)^2},\tag{4}$$

Eq. (4) computes the KL divergence without calculating any integral, which is computationally cost-efficient. Besides, the computation of profile dissimilarity can be performed under the Homomorphic Encryption for minimum knowledge disclosure [56] (see Appendix D for details).

²Fused representations refer to the sum of elements in the original representations produced by a single layer (channel-wise for a residual block).

IV. THE TRAINING ALGORITHM FEDPROF

Our research aims to optimize the global model over a large group of clients (datasets) of disparate training value. Given the client set U(|U|=N), let D_k denote the local dataset on client k and D^* the validation set on the server, We formulate the optimization problem in (5) where the coefficient ρ_k differentiates the importance of the local objective functions $F_k(w)$ and depends on the data in D_k . Our global objective is in a sense similar to the agnostic learning scenario [33] where a non-uniform mixture of local data distributions is implied.

$$\arg\min_{w} F(w) = \sum_{k=1}^{N} \rho_k F_k(w), \tag{5}$$

where w is the parameter set of the global model. The coefficients $\{\rho_k\}_{k=1}^N$ add up to 1. $F_k(w)$ is client k's local objective function of training based on the loss function $\ell(\cdot)$:

$$F_k(w) = \frac{1}{|D_k|} \sum_{(x_i, y_i) \in D_k} \ell(x_i, y_i; w),$$
(6)

Involving the "right" clients facilitates the convergence. With this motivation we score each client with λ_k each round based on the representation profile dissimilarity:

$$\lambda_k = \exp(-\alpha \cdot div(RP_k(v_k), RP^*(v_k)), \tag{7}$$

where v_k is the version of RP_k (i.e., the version of the global model that client k receives) and α is a preference factor deciding how biased the selection strategy needs to be towards the clients with small profile dissimilarity (i.e., higher training value). With $\alpha = 0$, our strategy is equivalent to random selection. The scores connect the representation profiling and matching scheme to the design of selective client participation strategy adopted in our FL training algorithm FEDPROF, which is outlined in Algorithm 1 (see Appendix B for a detailed version with both client and server processes).

Algorithm 1: the FEDPROF algorithm

```
Input: max rounds T_{max}, local iterations E, fraction C
 1 Initialize global model w and generate baseline profile RP^*
2 Collect initial representation profiles \{RP_k\}_{k\in U} from all clients
   for round T \leftarrow 1 to T_{max} do
        Update client scores \{\lambda_k\}_{k\in U} and compute \Lambda = \sum_{k\in U} \lambda_k
 3
        S(T) \leftarrow \text{Choose } K = N \cdot C \text{ clients by probability distribution } \{\frac{\lambda_k}{\Lambda}\}_{k \in U}
       for client k in S(T) in parallel do
            RP_k \leftarrow updateProfile(k, w, T-1)
           w_k \leftarrow localTraining(k, w, E)
 6
       Collect local profiles from the clients in S(T)
 7
        Update w via model aggregation
       Evaluate w and update RP^*
   end
10 return w
```

The convergence rate of FL algorithms with opportunistic client selection (sampling) has been extensively studied in the literature [35][41]. Inspired by refs. [4][35], we present Theorem 1 to guarantee the convergence of our algorithm. Similar to refs. [61][62][35], we assume that $\{F_k\}_{k=1}^N$ are L-smooth and μ -strongly convex and that in expectation, the variance of local stochastic gradients are bounded by ϵ^2 and their squared norms are bounded by G^2 .

Theorem 1. Using partial aggregation and a strategy π that selects clients by the probabilities $\{q_k\}_{k=1}^N$ to form the set S(t), the global model w(t) converges in expectation by having $q_k = \rho_k$, an aggregation interval $E \geq 1$ and a decreasing step size (learning rate) $\eta_t = \frac{2}{\mu(t+\gamma)}$.

$$E_{S(t)}[F(w(t))] - F^* \le \frac{L}{(\gamma + t)} \left(\frac{2(\mathcal{B} + \mathcal{C})}{\mu^2} + \frac{\gamma + 1}{2} \Delta_1 \right), \tag{8}$$

where
$$t \in T_A = \{nE | n = 1, 2, ...\}$$
, $\gamma = \max\{\frac{8L}{\mu}, E\} - 1$, $\mathcal{B} = \sum_{k=1}^N \rho_k^2 \epsilon_k^2 + 6L\Gamma + 8(E-1)^2 G^2$, $\mathcal{C} = \frac{4}{K} E^2 G^2$, $\Gamma = F^* - \sum_{k=1}^N \rho_k F_k^*$, $\Delta_1 = \mathbb{E} \|\bar{w}(1) - w^*\|^2$, and $K = |S(t)| = N \cdot C$.

The proof of Theorem 1 is provided in Appendix C.

V. EXPERIMENTS

We conducted extensive experiments to evaluate FEDPROF under various FL settings. Apart from FEDAVG [2], we also reproduced several state-of-the-art FL algorithms for comparison. For fair comparison, the algorithms are grouped by the aggregation method (i.e., full aggregation and partial aggregation) and configured following the hyper-parameter settings in their papers (if any). Table I summarizes these FL algorithms. Note that our algorithm can adapt to both aggregation methods.

TABLE I: The implemented FL algorithms for comparison

Algorithm	Aggregation method	Rule of selection
FEDAVG [2]	full aggregation	random selection
CFCFM [27]	full aggregation	submission order
FEDAVG-RP	partial (Scheme II, [35])	random selection
FedProx [36]	partial aggregation	weighted random by data ratio
FEDADAM [34]	partial with momentum	random selection
AFL [50]	partial with momentum	local loss valuation
FEDPROF (ours)	full/partial aggregation	weighted random by score

A. Experiment Setup

We built our simulated FL system and implemented the algorithms based on the Pytorch framework (Build 1.7.0). We first set up a Small-scale Task (S-Task) to learn a multi-layer feed-forward network model from decentralized sensor data for predicting carbon monoxide (CO) and nitrogen oxides (NOx) emissions using the *GasTurbine*³ dataset. Next, we set up a Large-scale Task (L-Task) to train a CNN over a large population of user devices for image classification (*EMNIST*⁴). In both tasks, data sharing is not allowed between any parties. The data are non-IID across the end devices.⁵ We introduce a diversity of noise into the local datasets on end devices to simulate the discrepancy in data quality. The S-Task is performed over 50 sensor clients and 50% of them produce noisy data (including 10% invalid). The population for L-Task contains 1000 end devices across which the data spread with strong class imbalance – roughly 60% of the samples on each device fall into the same class. 15% of the local datasets in the L-Task are irrelevant images whereas another 45% of them are low-quality images (blurred or affected by salt-and-pepper noise). Considering the population of the clients, the setting of the selection fraction *C* is based on the scale of the training participants suggested in ref. [5]. For both tasks, the clients are heterogeneous in terms of both performance and communication bandwidth. More experimental settings are listed in Table IV in Appendix E where the environment setup is also given in details.

³https://archive.ics.uci.edu/ml/datasets/Gas+Turbine+CO+and+NOx+Emission+Data+Set

⁴https://www.nist.gov/itl/products-and-services/emnist-dataset. We use the digits subset of EMNIST.

⁵In the S-Task, local datasets are of different sizes that follow a Gaussian distribution. In the L-Task, local data are largely imbalanced. Around 60% of the samples on each client have the same class label.

B. Evaluation Results

We evaluate the performance of our FEDPROF algorithm in terms of the efficacy (best accuracy achieved) and efficiency (costs for convergence) in establishing a global model for the two tasks. Tables II and III summarize the results. Figs. 3 and 4 plot the accuracy traces from the round-wise evaluations of the global model.

TABLE II: The results of running the S-Task. The best accuracy is achieved by running for long enough. Other metrics are recorded when reaching the targeted accuracy (80% for the S-Task).

			Full a	ggregation	1				
	C=0.2					C=0.3			
	Best acc	For accuracy@0.8			Best acc	For accuracy@0.8			
		Rounds	Time(s)	E(Wh)	Best acc	Rounds	Time(s)	E(Wh)	
FEDAVG	0.805	56	2869.66	2.87	0.806	52	3160.01	4.12	
CFCFM	0.806	39	1230.81	1.61	0.802	42	1495.34	2.91	
Ours	0.824	16	803.74	0.80	0.827	12	701.18	0.94	
	Partial aggregation								
	C=0.2								
	Best acc	For accuracy@0.8			D4	For accuracy@0.8			
	Best acc	Rounds	Time(s)	E(Wh)	Best acc	Rounds	Time(s)	E(Wh)	
FEDAVG-RP	0.819	13	735.48	0.71	0.817	8	466.90	0.64	
FEDPROX	0.821	16	899.93	0.79	0.810	16	841.65	1.08	
FEDADAM	0.818	8	438.20	0.42	0.819	12	667.00	0.94	
AFL	0.816	6	313.81	0.30	0.813	6	298.81	0.42	
Ours	0.844	5	283.76	0.27	0.841	4	235.22	0.35	

TABLE III: The results of running the L-Task. The best accuracy is achieved by running for long enough. Other metrics are recorded when reaching the targeted accuracy (90% for the L-Task).

			Full ag	gregation				
	C=0.05					C=0.1		
Best acc	For accuracy@0.9			Best acc	For accuracy@0.9			
	best acc	Rounds	Time(s)	E(Wh)	best acc	Rounds	Time(s)	E(Wh)
FEDAVG	0.906	213	10407.30	60.01	0.929	76	3894.26	43.16
CFCFM	0.923	251	8645.17	61.37	0.932	75	2675.56	37.62
Ours	0.926	98	4846.15	28.22	0.945	45	2295.03	25.98
Partial aggregation								
C=0.05								
	Best acc	For accuracy@0.9			D 4	For accuracy@0.9		
	best acc	Rounds	Time(s)	E(Wh)	Best acc	Rounds	Time(s)	E(Wh)
FEDAVG-RP	0.937	12	572.90	3.29	0.938	12	603.94	6.57
FEDPROX	0.936	13	640.01	3.58	0.942	11	559.16	5.91
FEDADAM	0.940	12	599.96	3.47	0.939	12	608.85	6.76
AFL	0.952	10	479.73	2.73	0.944	9	476.62	5.26
Ours	0.962	8	383.94	2.26	0.962	8	413.16	4.64

- 1) Convergence in different aggregation modes: Our results show a great difference in convergence rate under different aggregation modes. From Figs. 3 and 4, we observe that partial aggregation facilitates faster convergence of the global model than full aggregation, which is consistent with the observations made by [35]. Our FEDPROF algorithm yields the fastest convergence in both groups of comparison for both tasks because selective participation benefits both aggregation methods.
- 2) Best accuracy of the global model: Through the training process of FL, the global model is evaluated each round on the server. The best global model obtained thus far is stored on the server. As shown in the 2nd column of Tables II and III, our FEDPROF algorithm improves the accuracy achieved by 2.5% when compared against the baselines (FEDAVG and FEDAVG-RP). The AFL algorithm uses a loss-oriented client selection strategy, which shows the closest performance to our algorithm in the L-Task but the worst accuracy in the S-Task.
- 3) Total communication rounds for convergence: The communication cost for convergence is a key indicator to the efficiency of FL. In the S-Task, our algorithm takes less than half the communication rounds required by

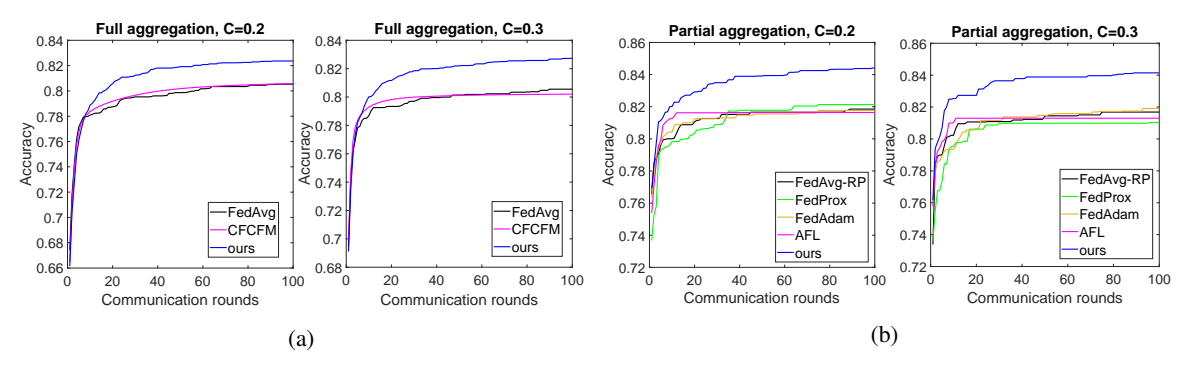


Fig. 3: The traces of evaluation accuracy of the global model through 100 rounds in the S-Task using (a) the full-aggregation method, and (b) the partial-aggregation method.

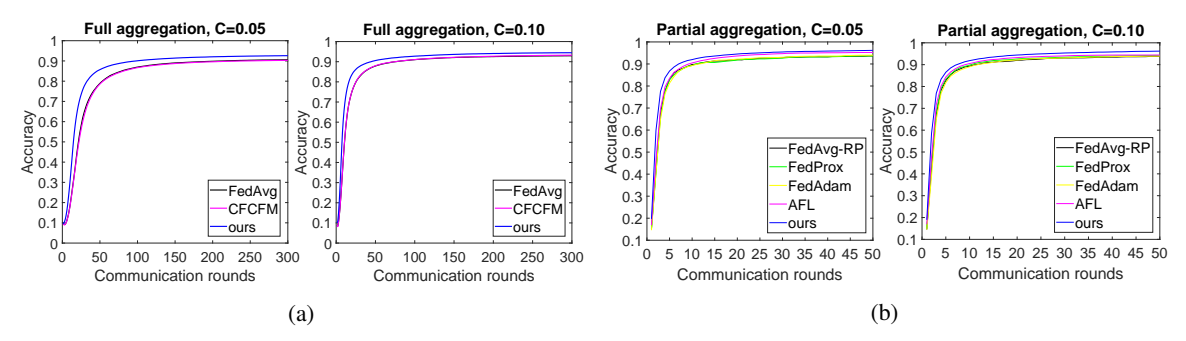


Fig. 4: The traces of evaluation accuracy of the global model in the L-Task using (a) the full-aggregation method (through 300 rounds), and (b) the partial aggregation method (through 50 rounds).

other algorithms in most cases. In the L-Task with C=0.05, our algorithm reaches 90% accuracy within 100 rounds whilst FEDAVG and CFCFM need more than 200. In this case, FEDPROF also achieves approximately 7% higher accuracy in 50 rounds. The partial aggregation method turns out to be much more communication-efficient: our algorithm only needs 5 and 8 times of communication to reach the target accuracy for S-task and L-task, respectively.

- 4) Total time needed for convergence: The overall time consumption is closely related to total communication rounds needed for convergence and the time cost for each round. Algorithms requiring more rounds to converge typically take longer to reach the accuracy target except the case of CFCFM, which priorities the clients that work faster. Using FEDAVG as the baseline, CFCFM accelerates the training process by 2.1x whist our algorithm provides a 4.5x speedup for achieving the same target accuracy (S-Task, C=0.3). FEDPROF also has a clear advantage over FEDAVG-RP, FEDPROX and FEDADAM in the partial aggregation group where it shows a 2.6x speedup over FEDAVG-RP in the S-Task with C=0.2.
- 5) Energy consumption of end devices: A main concern for the end devices, as the participants of FL, is their power usage (Watt hours). Full aggregation methods experience slower convergence and thus endure higher energy cost on the devices. For example, with a small selection fraction C=0.05 in the L-Task, FEDAVG and CFCFM consume over 60Wh to reach the target accuracy. In this case, our algorithm reduces the cost by more than a half (28.22Wh). With the partial aggregation mode, the reduction by our algorithm is up to 62% (S-Task, C = 0.2). Considering all the cases, FEDPROF achieves the target accuracy with the least energy cost, providing an reduction of 29% \sim 53%.
- 6) Differentiated participation with FEDPROF: Fig. 5 reflects the preference of our selection strategy. In the S-Task we can observe that the clients with useless samples or noisy data get significantly less involved (<10 on average) in training. In the L-Task our algorithm also effectively limits (basically excludes) the clients who owns the image data of poor quality (i.e., irrelevant or severely blurred), whereas the clients

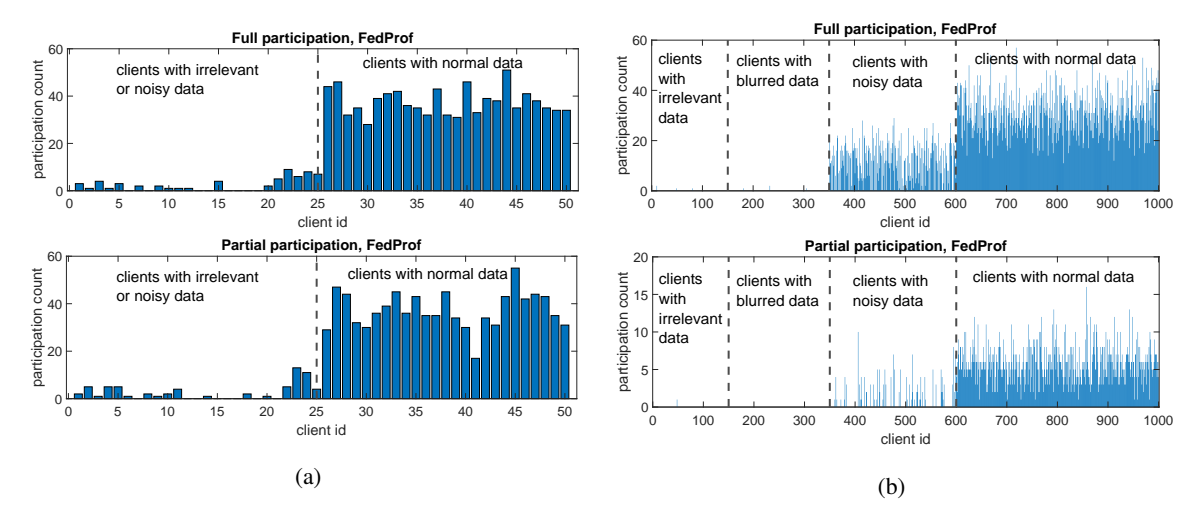


Fig. 5: Total counts by client of participation (i.e., being selected) in (a) the S-Task and (b) the L-Task. For clarity, clients are indexed according to their local data quality.

with moderately noisy images are selected with reduced frequency as compared to those with normal data. A potential issue of having the preference towards some of the devices is about fairness. Nonetheless, one can apply our algorithm together with an incentive mechanism (e.g., [59]) to address it.

VI. CONCLUSION

Federated learning provides a privacy-preserving approach to decentralized training but is vulnerable to the heterogeneity and uncertain quality of on-device data. In this paper, we use a novel approach to address the issue without violating the data locality restriction. We first provide key insights for the distribution of data representations and develop a dynamic data representation profiling and matching scheme. Based on the scheme we propose a selective FL training algorithm FEDPROF that adaptively adjusts clients' participation chance based on their profile dissimilarity. Evaluation results show a significant improvement in efficiency and reduction of costs for convergence using our algorithm.

REFERENCES

- [1] Robert van der Meulen. What Edge Computing Means for Infrastructure and Operations Leaders. [Online]. Available: https://www.gartner.com/smarterwithgartner/what-edge-computing-means-for-infrastructure-and-operations-leaders/
- [2] McMahan, B., Moore, E., Ramage, D., Hampson, S., & y Arcas, B. A. (2017, April). Communication-efficient learning of deep networks from decentralized data. In Artificial Intelligence and Statistics (pp. 1273-1282). PMLR.
- [3] Konečný, J., McMahan, H. B., Yu, F. X., Richtárik, P., Suresh, A. T., & Bacon, D. (2016). Federated learning: Strategies for improving communication efficiency. arXiv preprint arXiv:1610.05492.
- [4] Wang, S., Tuor, T., Salonidis, T., Leung, K. K., Makaya, C., He, T., & Chan, K. (2019). Adaptive federated learning in resource constrained edge computing systems. IEEE Journal on Selected Areas in Communications, 37(6), 1205-1221.
- [5] Kairouz, P., McMahan, H. B., Avent, B., Bellet, A., Bennis, M., Bhagoji, A. N., ... & Zhao, S. (2019). Advances and open problems in federated learning. arXiv preprint arXiv:1912.04977.
- [6] Wu, W., He, L., Lin, W., & Mao, R. (2020). Accelerating Federated Learning over Reliability-Agnostic Clients in Mobile Edge Computing Systems. IEEE Transactions on Parallel and Distributed Systems.
- [7] Hard, A., Rao, K., Mathews, R., Ramaswamy, S., Beaufays, F., Augenstein, S., ... & Ramage, D. (2018). Federated learning for mobile keyboard prediction. arXiv preprint arXiv:1811.03604.
- [8] Bhagoji, A. N., Chakraborty, S., Mittal, P., & Calo, S. (2019, May). Analyzing federated learning through an adversarial lens. In International Conference on Machine Learning (pp. 634-643). PMLR.
- [9] Bagdasaryan, E., Veit, A., Hua, Y., Estrin, D., & Shmatikov, V. (2020, June). How to backdoor federated learning. In International Conference on Artificial Intelligence and Statistics (pp. 2938-2948). PMLR.
- [10] Lin, W. C., Tsai, C. F., Hu, Y. H., & Jhang, J. S. (2017). Clustering-based undersampling in class-imbalanced data. Information Sciences, 409, 17-26.
- [11] Cui, Y., Jia, M., Lin, T. Y., Song, Y., & Belongie, S. (2019). Class-balanced loss based on effective number of samples. In Proceedings of the IEEE/CVF Conference on Computer Vision and Pattern Recognition (pp. 9268-9277).

- [12] Fang, M., Cao, X., Jia, J., & Gong, N. (2020). Local model poisoning attacks to byzantine-robust federated learning. In 29th USENIX Security Symposium (USENIX Security 20) (pp. 1605-1622).
- [13] Tolpegin, V., Truex, S., Gursoy, M. E., & Liu, L. (2020, September). Data poisoning attacks against federated learning systems. In European Symposium on Research in Computer Security (pp. 480-501). Springer, Cham.
- [14] Yoo, J., Ahn, N., & Sohn, K. A. (2020). Rethinking data augmentation for image super-resolution: A comprehensive analysis and a new strategy. In Proceedings of the IEEE/CVF Conference on Computer Vision and Pattern Recognition (pp. 8375-8384).
- [15] Yu, D., Zhang, H., Chen, W., Yin, J., & Liu, T. Y. (2021, May). How Does Data Augmentation Affect Privacy in Machine Learning?. In Proceedings of the AAAI Conference on Artificial Intelligence (Vol. 35, No. 12, pp. 10746-10753).
- [16] Feelders, A. J. (1996, January). Learning from Biased Data Using Mixture Models. In KDD (pp. 102-107).
- [17] Bengio, Y., Courville, A., & Vincent, P. (2013). Representation learning: A review and new perspectives. IEEE transactions on pattern analysis and machine intelligence, 35(8), 1798-1828.
- [18] Morcos, A. S., Raghu, M., & Bengio, S. (2018). Insights on representational similarity in neural networks with canonical correlation. arXiv preprint arXiv:1806.05759.
- [19] Kornblith, S., Norouzi, M., Lee, H., & Hinton, G. (2019, May). Similarity of neural network representations revisited. In International Conference on Machine Learning (pp. 3519-3529). PMLR.
- [20] Li, Q., He, B., & Song, D. (2021). Model-Contrastive Federated Learning. In Proceedings of the IEEE/CVF Conference on Computer Vision and Pattern Recognition (pp. 10713-10722).
- [21] Feng, S., & Yu, H. (2020). Multi-participant multi-class vertical federated learning. arXiv preprint arXiv:2001.11154.
- [22] Alistarh, D., Grubic, D., Li, J., Tomioka, R., & Vojnovic, M. (2017). QSGD: Communication-efficient SGD via gradient quantization and encoding. In Advances in Neural Information Processing Systems (pp. 1709-1720).
- [23] Wu, J., Huang, W., Huang, J., & Zhang, T. (2018, July). Error Compensated Quantized SGD and its Applications to Large-scale Distributed Optimization. In Proceedings of the International Conference on Machine Learning (pp. 5321-5329).
- [24] Zheng, S., Meng, Q., Wang, T., Chen, W., Yu, N., Ma, Z. M., & Liu, T. Y. (2017, July). Asynchronous stochastic gradient descent with delay compensation. In International Conference on Machine Learning (pp. 4120-4129). PMLR.
- [25] Yang, H., Fang, M., & Liu, J. (2021, September). Achieving Linear Speedup with Partial Worker Participation in Non-IID Federated Learning. In International Conference on Learning Representations.
- [26] Niknam, S., Dhillon, H. S., & Reed, J. H. (2020). Federated learning for wireless communications: Motivation, opportunities, and challenges. IEEE Communications Magazine, 58(6), 46-51.
- [27] Wu, W., He, L., Lin, W., Mao, R., Maple, C., & Jarvis, S. A. (2020). SAFA: a Semi-Asynchronous Protocol for Fast Federated Learning with Low Overhead. IEEE Transactions on Computers.
- [28] Cui, L., Su, X., Zhou, Y., & Pan, Y. (2021). Slashing Communication Traffic in Federated Learning by Transmitting Clustered Model Updates. IEEE Journal on Selected Areas in Communications.
- [29] Luping, W. A. N. G., Wei, W. A. N. G., & Bo, L. I. (2019, July). CMFL: Mitigating communication overhead for federated learning. In 2019 IEEE 39th International Conference on Distributed Computing Systems (ICDCS) (pp. 954-964). IEEE.
- [30] Tan, A. Z., Yu, H., Cui, L., & Yang, Q. (2021). Towards personalized federated learning. arXiv preprint arXiv:2103.00710.
- [31] Deng, Y., Kamani, M. M., & Mahdavi, M. (2020). Adaptive personalized federated learning. arXiv preprint arXiv:2003.13461.
- [32] Fallah, A., Mokhtari, A., & Ozdaglar, A. (2020). Personalized federated learning with theoretical guarantees: A model-agnostic meta-learning approach. Advances in Neural Information Processing Systems, 33, 3557-3568.
- [33] Mohri, M., Sivek, G., & Suresh, A. T. (2019, May). Agnostic federated learning. In International Conference on Machine Learning (pp. 4615-4625). PMLR.
- [34] Leroy, D., Coucke, A., Lavril, T., Gisselbrecht, T., & Dureau, J. (2019, May). Federated learning for keyword spotting. In ICASSP 2019-2019 IEEE International Conference on Acoustics, Speech and Signal Processing (ICASSP) (pp. 6341-6345). IEEE.
- [35] Li, X., Huang, K., Yang, W., Wang, S., & Zhang, Z. (2019). On the convergence of fedayg on non-iid data. arXiv preprint arXiv:1907.02189.
- [36] Li, T., Sahu, A. K., Zaheer, M., Sanjabi, M., Talwalkar, A., & Smith, V. (2018). Federated optimization in heterogeneous networks. arXiv preprint arXiv:1812.06127.
- [37] Nishio, T., & Yonetani, R. (2019, May). Client selection for federated learning with heterogeneous resources in mobile edge. In ICC 2019-2019 IEEE International Conference on Communications (ICC) (pp. 1-7). IEEE.
- [38] Wang, J., Liu, Q., Liang, H., Joshi, G., & Poor, H. V. (2020). Tackling the objective inconsistency problem in heterogeneous federated optimization. arXiv preprint arXiv:2007.07481.
- [39] Chai, Z., Fayyaz, H., Fayyaz, Ž., Anwar, A., Zhou, Y., Baracaldo, N., ... & Cheng, Y. (2019). Towards taming the resource and data heterogeneity in federated learning. In 2019 USENIX Conference on Operational Machine Learning (OpML 19) (pp. 19-21).
- [40] Acar, D. A. E., Zhao, Y., Matas, R., Mattina, M., Whatmough, P., & Saligrama, V. (2021, September). Federated learning based on dynamic regularization. In International Conference on Learning Representations.
- [41] Chen, W., Horvath, S., & Richtarik, P. (2020). Optimal client sampling for federated learning. arXiv preprint arXiv:2010.13723.
- [42] Shi, W., Zhou, S., & Niu, Z. (2020, June). Device scheduling with fast convergence for wireless federated learning. In ICC 2020-2020 IEEE International Conference on Communications (ICC) (pp. 1-6). IEEE.
- [43] Chen, M., Poor, H. V., Saad, W., & Cui, S. (2020). Convergence time optimization for federated learning over wireless networks. IEEE Transactions on Wireless Communications, 20(4), 2457-2471.
- [44] Chen, M., Shlezinger, N., Poor, H. V., Eldar, Y. C., & Cui, S. (2021). Communication-efficient federated learning. Proceedings of the National Academy of Sciences, 118(17).
- [45] Chai, Z., Ali, A., Zawad, S., Truex, S., Anwar, A., Baracaldo, N., ... & Cheng, Y. (2020, June). Tifl: A tier-based federated learning system. In Proceedings of the 29th International Symposium on High-Performance Parallel and Distributed Computing (pp. 125-136).
- [46] Wang, H., Kaplan, Z., Niu, D., & Li, B. (2020, July). Optimizing federated learning on non-iid data with reinforcement learning. In IEEE INFOCOM 2020-IEEE Conference on Computer Communications (pp. 1698-1707). IEEE.
- [47] Lai, F., Zhu, X., Madhyastha, H. V., & Chowdhury, M. (2021, July). Oort: Efficient federated learning via guided participant selection. In 15th USENIX Symposium on Operating Systems Design and Implementation (OSDI 21) (pp. 19-35).

- [48] Sarkar, D., Narang, A., & Rai, S. (2020). Fed-Focal Loss for imbalanced data classification in Federated Learning. arXiv preprint arXiv:2011.06283.
- [49] Tuor, T., Wang, S., Ko, B. J., Liu, C., & Leung, K. K. Overcoming Noisy and Irrelevant Data in Federated Learning. arXiv preprint arXiv:2001.08300.
- [50] Goetz, J., Malik, K., Bui, D., Moon, S., Liu, H., & Kumar, A. (2019). Active Federated Learning. arXiv preprint arXiv:1909.12641.
- [51] Cho, Y. J., Wang, J., & Joshi, G. (2020). Client Selection in Federated Learning: Convergence Analysis and Power-of-Choice Selection Strategies. arXiv preprint arXiv:2010.01243.
- [52] Tran, N. H., Bao, W., Zomaya, A., Nguyen, M. N., & Hong, C. S. (2019, April). Federated learning over wireless networks: Optimization model design and analysis. In IEEE INFOCOM 2019-IEEE Conference on Computer Communications (pp. 1387-1395). IEEE.
- [53] Roberts, S. J., & Penny, W. D. (2002). Variational Bayes for generalized autoregressive models. IEEE Transactions on Signal Processing, 50(9), 2245-2257.
- [54] Lemons, D. S., & Langevin, P. (2002). An introduction to stochastic processes in physics. The Johns Hopkins University Press, p. 34, ISBN 0-8018-6866-1.
- [55] Billingsley, P. Probability and Measure, 2nd ed. New York: p. 371, Wiley, 1986.
- [56] Gentry, C. (2009, May). Fully homomorphic encryption using ideal lattices. In Proceedings of the forty-first annual ACM symposium on Theory of computing (pp. 169-178).
- [57] Song, J., Li, T., Wang, Z., & Zhu, Z. (2013). Study on energy-consumption regularities of cloud computing systems by a novel evaluation model. Computing, 95(4), 269-287.
- [58] Carroll, A., & Heiser, G. (2010, June). An Analysis of Power Consumption in a Smartphone. In Proceedings of the 2010 USENIX conference on USENIX annual technical conference (pp. 1-14). Boston, MA.
- [59] Yu, H., Liu, Z., Liu, Y., Chen, T., Cong, M., Weng, X., ... & Yang, Q. (2020, February). A fairness-aware incentive scheme for federated learning. In Proceedings of the AAAI/ACM Conference on AI, Ethics, and Society (pp. 393-399).
- [60] He, K., Zhang, X., Ren, S., & Sun, J. (2016). Deep residual learning for image recognition. In Proceedings of the IEEE conference on computer vision and pattern recognition (pp. 770-778).
- [61] Stich, S. U., Cordonnier, J. B., & Jaggi, M. (2018). Sparsified SGD with Memory. Advances in Neural Information Processing Systems, 31, 4447-4458.
- [62] Zhang, Y., Duchi, J. C., & Wainwright, M. J. (2013). Communication-efficient algorithms for statistical optimization. The Journal of Machine Learning Research, 14(1), 3321-3363.

APPENDIX A PROOF OF PROPOSITIONS

A. Proof of Proposition 1

Without loss of generality, we provide the proof of Proposition 1 for the pre-activation representations from dense (fully-connected) layers and standard convolutional layers, respectively. The results can be easily extended to other linear neural operators.

Dense layers

Proof. Let $\Omega = \{neu_1, neu_2, ..., neu_q\}$ denote a dense layer (with q neurons) of any neural network model and H_k denote the pre-activation output of neu_k in Ω . We first provide the theoretical proof to support the observation that H_k tends to follow the Gaussian distribution.

Let $\chi = \mathbb{R}^v$ denote the input feature space (with v features) and assume the feature X_i (which is a random variable) follows a certain distribution $\zeta_i(\mu_i, \sigma_i^2)$ (not necessarily Gaussian) with finite mean $\mu_i = \mathrm{E}[X_i]$ and variance $\sigma_i^2 = \mathrm{E}[X_i - \mu_i]$. For each neuron neu_k , let $\mathbf{w}_k = [w_{k,1} \, w_{k,2} \dots w_{k,v}]$ denote the neuron's weight vector, b_k denote the bias, and $Z_{k,i} = X_i w_{k,i}$ denote the i-th weighted input. Let H_k denote the output of neu_k . During the forward propagation, we have:

$$H_k = X \boldsymbol{w}_k^T + b_k$$

$$= \sum_{i=1}^{v} X_i w_{k,i} + b_k$$

$$= \sum_{i=1}^{v} Z_{k,i} + b_k.$$
(9)

Apparently $Z_{k,i}$ is a random variable because $Z_{k,i} = X_i w_{k,i}$ (where the weights $w_{k,i}$ are constants during a forward pass), thus H_k is also a random variable according to Eq. (9).

In an ideal situation, the inputs variables X_1, X_2, \ldots, X_v may follow a multivariate Gaussian distribution, in which case Proposition 1 automatically holds due to the property of multivariate normal distribution that every linear combination of the components of the random vector $(X_1, X_2, \ldots, X_v)^T$ follows a Gaussian distribution [54]. In other words, $H_k = X_1 w_{k,1} + X_2 w_{k,2} + \ldots + X_v w_{k,v} + b_k$ is a normally distributed variable since $w_{k,i}$ and b_k $(k=1,2,\ldots,v)$ are constants in the forward propagation. A special case for this condition is that X_1, X_2, \ldots, X_v are independent on each other and X_i follows a Gaussian distribution $\mathcal{N}(\mu_i, \sigma_i^2)$ for all $i=1,2,\ldots,v$. In this case, by the definition of $Z_{k,i}$, we have:

$$Z_{k,i} = X_i w_{k,i} \sim \mathcal{N}(w_{k,i} \mu_i, (w_{k,i} \sigma_i)^2), \tag{10}$$

where Z_1, Z_2, \dots, Z_v are independent on each other. Combining Eqs. (9) and (10), we have:

$$H_k \sim \mathcal{N}\left(\sum_{i=1}^{v} w_{k,i} \mu_i + b_k, \sum_{i=1}^{v} (w_{k,i} \sigma_i)^2\right),$$
 (11)

For more general cases where X_1, X_2, \ldots, X_v are not necessarily normally distributed, we assume the weighted inputs $Z_{k,i}$ of the dense layer satisfy the Lyapunov's condition (see *definition* 1). As a result, we have the following according to the Central Limit Theorem (CLT) [55] considering that X_i follows $\zeta_i(\mu_i, \sigma_i^2)$:

$$\frac{1}{s_k} \sum_{i=1}^{v} \left(Z_{k,i} - w_{k,i} \mu_i \right) \xrightarrow{d} \mathcal{N}(0,1)$$
(12)

where $s_k = \sqrt{\sum_{i=1}^v \left(w_{k,i}\sigma_i\right)^2}$ and $\mathcal{N}(0,1)$ denotes the standard normal distribution. Equivalently, for every neu_k we have:

$$\sum_{i=1}^{v} Z_{k,i} \xrightarrow{d} \mathcal{N}(\sum_{i=1}^{v} w_{k,i} \mu_i, s_k^2)$$
(13)

Combining Eqs. (9) and (13) we can derive that:

$$H_k \xrightarrow{d} \mathcal{N}(\sum_{i=1}^v w_{k,i}\mu_i + b_k, s_k^2),$$
 (14)

which means that $H_k(k=1,2,\ldots,v)$ tend to follow Gaussian distribution and proves our Proposition 1 for fully-connected layers.

Convolutional layers

Proof. Standard convolution in CNNs is also a linear transformation of the input feature space and its main difference from dense layers rests on the restricted size of receptive field. Without loss of generality, we analyze the representation (output) of a single kernel. To facilitate our analysis for convolutional layers, let C denote the number of input channels and K denote the kernel size. For ease of presentation, we define a receptive field mapping function $\Theta(k,i,j)$ that maps the positions (k for channel index, i and j for indices on the same channel) of elements in the feature map (i.e., the representations) to the input features. For the k-th kernel, let W_k denote its weight tensor (with $W_{k,c}$ being the weight matrix for channel c) and b_k its bias.

Given the corresponding input patch $X_{\Theta(k,i,j)}$, The element $H_{k,i,j}$ of the representations from a convolutional layer can be formulated as:

$$H_{k,i,j} = \sum_{c=1}^{C} \sum_{i'=1}^{K} \sum_{j'=1}^{K} \left(X_{\Theta(k,i,j)} \circ W_{k,c} \right)_{i',j'} + b_k, \tag{15}$$

where o denotes Hadamard product. The three summations reduce the results of element-wise product between the input patch and the k-th kernel to the correspond representation element $H_{k,i,j}$ in the feature map. For ease of presentation, here we use the notation $Z_{c,i',j'}^{(k)}$ to replace $(X_{\Theta(k,i,j)} \circ W_{k,c})_{i',j'}$ and let $\zeta(\mu_{c,i',j'},\sigma_{c,i',j'}^2)$ be the distribution that $Z_{c,i',j'}^{(k)}$ follows. Note that ζ can be any distribution since we do not make any distributional assumption on $Z_{c,i',j'}^{(k)}$.

With the potations Eq. (15) can be rewritten in a circle form to $F_{c,i',j'}$.

With the notations, Eq. (15) can be rewritten in a similar form to Eq. (9):

$$H_{k,i,j} = \sum_{c=1}^{C} \sum_{i'=1}^{K} \sum_{j'=1}^{K} Z_{c,i',j'}^{(k)} + b_k.$$
(16)

We use the condition that the random variables $Z_{c,i',j'}^{(k)}$ satisfy the Lyapunov's condition, i.e., there exists a δ such that

$$\lim_{C \times K^2 \to \infty} \frac{1}{s^{2+\delta}} \sum_{c=1}^{C} \sum_{i'=1}^{K} \sum_{j'=1}^{K} E\left[|Z_{c,i',j'}^{(k)} - \mu_{c,i',j'}|^{2+\delta} \right] = 0, \tag{17}$$

where $s = \sqrt{\sum_{c=1}^C \sum_{i'=1}^K \sum_{j'=1}^K \sigma_{c,i',j'}^2}$. Then according to the Lyapunov CLT, the following holds:

$$H_{k,i,j} \xrightarrow{d} \mathcal{N}\left(\sum_{c,i',j' \in \Theta(k,i,j)} \mu_{c,i',j'} + b_k, \sum_{c,i',j' \in \Theta(k,i,j)} \sigma_{c,i',j'}^2\right), \tag{18}$$

which proves our Proposition 1 for standard convolution layers

B. Proof of Proposition 2

Without loss of generality, we prove Proposition 2 for the fused representations from the LSTM layer and the residual block of ResNet models, respectively. The results can be easily extended to other non-linear neural operators.

LSTM

Proof. Long Short-Term Memory (LSTM) models are popular for extracting useful representations from sequence data for tasks such as speech recognition and language modeling. Each LSTM layer contains multiple neural units. For the k-th unit, it takes as input the current input feature vector $X_t = (X_{t,1}, t_t, \ldots)$, hidden state vector H_{t-1} and its cell state $c_{t-1,k}$. The outputs of the unit are its new hidden state $h_{t,k}$ and cell state $h_{t,k}$ and this paper, we study the distribution of $h_{t,k}$. Multiple gates are adopted in an LSTM unit: by $h_{t,k}$, $h_{t,k}$,

$$i_{t,k} = \operatorname{sigmoid}(W_{(i)k}[H_{t-1}, X_t] + b_{(i)k}),$$

$$f_{t,k} = \operatorname{sigmoid}(W_{(f)k}[H_{t-1}, X_t] + b_{(f)k}),$$

$$g_{t,k} = \tanh(W_{(g)k}[H_{t-1}, X_t] + b_{(g)k}),$$

$$o_{t,k} = \operatorname{sigmoid}(W_{(o)k}[H_{t-1}, X_t] + b_{(o)k}),$$

$$c_{t,k} = f_{t,k} \cdot c_{t-1,k} + i_{t,k}g_{t,k},$$
(19)

where the $W_{(i)k}$, $W_{(f)k}$, $W_{(g)k}$ and $W_{(o)k}$ are the weight parameters and $b_{(i)k}$, $b_{(f)k}$, $b_{(g)k}$ and $b_{(o)k}$ are the bias parameters for the gates.

The output of the LSTM unit $h_{t,k}$ is calculated as the following:

$$h_{t,k} = o_{t,k} \cdot \tanh(c_{t,k}). \tag{20}$$

Using the final hidden state h(T, k) (with T being the length of the sequence) as the element of the layer-wise representation, we apply the following layer-wise fusion to further produce H over all the $h_{T,k}$ in a single LSTM layer:

$$H = \sum_{k=1}^{d} h_{T,k},\tag{21}$$

where d is the dimension of the LSTM layer. Again, by $\zeta(\mu_k, \sigma_k^2)$ we denote the distribution of $h_{T,k}$ (where the notation T is dropped here since it is typically a fixed parameter). With $\forall k=1,2,\ldots,d,\ h_{T,k}$ satisfying the Lyapunov's condition (defined in Proposition 1 with $Z_k=h_{T,k}$ in this case), by Central Limit Theorem H tends to follow the Gaussian distribution:

$$H \xrightarrow{d} \mathcal{N}(\sum_{i=1}^{d} \mu_k, \sum_{i=1}^{d} \sigma_k^2),$$
 (22)

which proves the Proposition 2 for layer-wise fused representations from LSTM.

Residual blocks

Proof. Residual blocks are the basic units in the Residual neural network (ResNet) architecture [60]. A typical residual block contains two convolutional layers with batch normalization (BN) and uses the ReLU activation function. The input of the whole block is added to the output of the second convolution (after BN) through a skip connection before the final activation. Since the convolution operators are the same as we formulate in the second part of Section A-A, here we use the notation $\Psi(X)$ to denote the sequential operations of convolution on X followed by BN, i.e., $\Psi(X) \triangleq BN(Conv(X))$. Again, we reuse the receptive field mapping $\Theta(k,i,j)$ as defined in Section A-A to position the inputs of the residual block corresponding to the element $Z_{k,i,j}$ in the output representation of the whole residual block.

Let X denote the input of the residual block and $Z_{k,i,j}$ denote an element in the output tensor of the whole residual block. Then we have:

$$Z_{k,i,j} = f\left(X_{k,i,j} + BN\left(Conv\left(f\left(BN\left(Conv\left(X_{\Theta(k,i,j)}\right)\right)\right)\right)\right)$$

$$= f\left(X_{k,i,j} + \Psi\left(f\left(\Psi\left(X_{\Theta(k,i,j)}\right)\right)\right)\right), \tag{23}$$

where f is the activation function (ReLU).

We perform channel-wise fusion on the representation from the residual block to produce H_k for the k-th channel:

$$H_k = \sum_{i=1}^{d_H} \sum_{j=1}^{d_W} Z_{k,i,j},\tag{24}$$

where d_H and d_{W} are the dimensions of the feature map and k is the channel index.

Let $\zeta(\mu_{k,i,j}, \sigma_{k,i,j}^2)$ denote the distribution that $Z_{k,i,j}$ follows. Then we apply the Lyapunov's condition to the representation elements layer-wise, i.e.,

$$\lim_{d_W \times d_H \to \infty} \frac{1}{s_k^{2+\delta}} \sum_{i=1}^{d_H} \sum_{j=1}^{d_W} \mathrm{E}\left[|Z_{k,i,j} - \mu_{k,i,j}|^{2+\delta} \right] = 0, \tag{25}$$

where $s_k = \sqrt{\sum_{i=1}^{d_H} \sum_{j=1}^{d_W} \sigma_{k,i,j}^2}$. With the above condition satisfied, by CLT H_k (the fused representation on channel k) tends to follow the Gaussian distribution:

$$H_k \xrightarrow{d} \mathcal{N}(\sum_{i=1}^{d_H} \sum_{j=1}^{d_W} \mu_{k,i,j}, \sum_{i=1}^{d_H} \sum_{j=1}^{d_W} \sigma_{k,i,j}^2),$$
 (26)

which proves the Proposition 2 for channel-wise fused representations from any residual block.

APPENDIX B

PSEUDO-CODE OF FEDPROF (DETAILED VERSION)

See Algorithm 2 for a complete version of the proposed training algorithm.

APPENDIX C CONVERGENCE ANALYSIS

In this section we provide the proof of the proposed Theorem 1. The analysis is mainly based on the results provided by ref. [35]. We first introduce several notations to facilitate the analysis.

A. Notations

Let U(|U|=N) denote the full set of clients and S(t)(|S(t)|=K) denote the set of clients selected for participating. By $w_k(t)$ we denote the local model on client k at time step t. We define an auxiliary sequence $v_k(t)$ for each client to represent the immediate local model after a local SGD update. Note that $v_k(t)$ is updated from $v_k(t-1)$ with learning rate η_{t-1} :

$$v_k(t) = w_k(t-1) - \eta_{t-1} \nabla F_k(w_k(t-1), \xi_{k,t-1}), \tag{27}$$

where $\nabla F_k(w_k(t-1), \xi_{k,t-1})$ is the stochastic gradient computed over a batch of data $\xi_{k,t-1}$ drawn from D_k with regard to $w_k(t-1)$.

We also define two virtual sequences $\bar{v}(t) = \sum_{k=1}^{N} \rho_k v_k(t)$ and $\bar{w}(t) = Aggregate(\{v_k(t)\}_{k=1}^{S(t)})$ for every time step t (Note that the actual global model w(t) is only updated at the aggregation steps $T_A = 0$ $\{E, 2E, 3E, \ldots\}$). Given an aggregation interval $E \ge 1$, we provide the analysis for the partial aggregation rule that yields $\bar{w}(t)$ as:

$$\bar{w}(t) = \frac{1}{K} \sum_{k \in S(t)} v_k(t),$$
 (28)

Algorithm 2: the FEDPROF protocol (detailed version)

```
Input: maximum number of rounds T_{max}, local iterations per round E, client set U, client fraction
              C, validation set D^*;
   Output: the global model w
   // Server process: running on the server
 1 Initialize global model w using a seed
 2 v \leftarrow 0 // version of the latest global model
 3 Broadcast the seed to all clients for identical model initialization
 4 Collect initial profiles \{RP_k\}_{k\in U} from all the clients
5 v_k \leftarrow 0, \forall k \in K
 6 Generate initial baseline profile RP^*(0) on D^*
7 K \leftarrow |U| \cdot C
   for round T \leftarrow 1 to T_{max} do
        Calculate div(RP_k(v_k), RP^*(v_k)) for each client k
 8
        Update client scores \{\lambda_k\}_{k\in U} and compute \Lambda = \sum_{k\in U} \lambda_k
        S(T) \leftarrow \text{Choose } K \text{ clients by probability distribution } \{\frac{\lambda_k}{\Lambda}\}_{k \in U}
10
        Distribute w to the clients in S(T)
11
       for client k in S(T) in parallel do
            v_k \leftarrow v, \, \forall k \in S(T)
12
            RP_k(v_k) \leftarrow updateProfile(k, w, v)
13
14
           w_k \leftarrow localTraining(k, w, E)
       end
       Collect local profiles from the clients in S(T)
15
       Update w via model aggregation
16
17
       Evaluate w and generate RP^*(v)
18
   end
19 return w
   // Client process: running on client k
   updateProfile(k, w, v):
        Generate RP_k on D_k with the global w received
20
21
        Label profile RP_k with version number v
22
       Return RP_k
   return
   localTraining(k, w, E):
       w_k \leftarrow w
23
       for step e \leftarrow 1 to E do
           Update w_k using gradient-based method
24
       end
       Return w_k
25
   return
```

where S(t) (|S(t)|=K) is the selected set of clients for the round $\lceil \frac{t}{E} \rceil$ that contains step t. At the aggregation steps T_A , w(t) is equal to $\bar{w}(t)$, i.e., $w(t)=\bar{w}(t)$ if $t\in T_A$.

To facilitate the analysis, we assume each client always performs model update (and synchronization) to produce $v_k(t)$ and $\bar{v}(t)$ (but obviously it does not affect the resulting \bar{w} and w for $k \notin S(t)$).

$$w_k(t) = \begin{cases} v_k(t), & \text{if } t \notin T_A \\ \bar{w}(t), & \text{if } t \in T_A \end{cases}$$
 (29)

For ease of presentation, we also define two virtual gradient sequences: $\bar{g}(t) = \sum_{k=1}^{N} \rho_k \nabla F_k(w_k(t))$ and $g(t) = \sum_{k=1}^{N} \rho_k \nabla F_k(w_k(t), \xi_{k,t})$. Thus we have $\mathrm{E}[g(t)] = \bar{g}(t)$ and $\bar{v}(t) = \bar{w}(t-1) + \eta_{t-1}g(t-1)$.

B. Assumptions

We formally make four assumptions to support our analysis of convergence. Assumptions 1 and 2 are standard in the literature [35][4][51] defining the convexity and smoothness properties of the objective functions. Assumptions 3 and 4 bound the variance of the local stochastic gradients and their squared norms in expectation, respectively. These two assumptions are also made in refs. [35].

Assumption 1. $F_1, F_2, ..., F_N$ are L-smooth, i.e., for any $k \in U$, x and y: $F_k(y) \leq F_k(x) + (y - x)^T \nabla F_k(x) + \frac{L}{2} ||y - x||_2^2$

It is obvious that the global objective F is also L-smooth as a linear combination of F_1, F_2, \ldots, F_N with $\rho_1, \rho_2, \ldots, \rho_N$ being the weights.

Assumption 2. F_1, F_2, \ldots, F_N are μ -strongly convex, i.e., for all $k \in U$ and any $x, y : F_k(y) \ge F_k(x) + (y-x)^T \nabla F_k(x) + \frac{\mu}{2} ||y-x||_2^2$

Assumption 3. The variance of local stochastic gradients on each device is bounded: For all $k \in U$, $\mathbb{E}\|\nabla F_k(w_k(t), \xi_{t,k}) - F_k(w_k(t))\|^2 \le \epsilon^2$

Assumption 4. The squared norm of local stochastic gradients on each device is bounded: For all $k \in U$, $\mathbb{E}\|\nabla F_k(w_k(t), \xi_{t,k})\|^2 \leq G^2$

C. Key Lemmas

To facilitate the proof of our main theorem, we first present several key lemmas.

Lemma 1 (Result of one SGD step). Under Assumptions 1 and 2 and with $\eta_t < \frac{1}{4L}$, for any t it holds true that

$$\mathbb{E}\|\bar{v}(t+1) - w^*\|^2 \le (1 - \eta_t \mu) \mathbb{E}\|\bar{w}(t) - w^*\|^2 + \eta_t^2 \mathbb{E}\|g_t - \bar{g}_t\|^2 + 6L\eta_t^2 \Gamma + 2\mathbb{E}\left[\sum_{k=1}^N \rho_k \|w_k(t) - \bar{w}(t)\|^2\right], (30)$$

where $\Gamma = F^* - \sum_{k=1}^N \rho_k F_k^*$.

Lemma 2 (Gradient variance bound). Under Assumption 3, one can derive that

$$\mathbb{E}\|g_t - \bar{g}_t\|^2 \le \sum_{k=1}^N \rho_k^2 \epsilon_k^2.$$
 (31)

Lemma 3 (Bounded divergence of $w_k(t)$). Assume Assumption 4 holds and a non-increasing step size η_t s.t. $\eta_t \leq 2\eta_{t+E}$ for all $t=1,2,\ldots$, it follows that

$$E\left[\sum_{k=1}^{N} \rho_k \|w_k(t) - \bar{w}(t)\|^2\right] \le 4\eta_t^2 (E - 1)^2 G^2.$$
(32)

Lemmas 1, 2 and 3 hold for both full and partial participation and are independent of the client selection strategy. We refer the readers to ref. [35] for their proofs and focus our analysis on opportunistic client selection.

The next two lemmas give important properties of the aggregated model \bar{w} as a result of partial participation and non-uniform client selection/sampling.

Lemma 4 (Unbiased aggregation). For any aggregation step $t \in T_A$ and with $q_k = \rho_k$ in the selection of S(t), it follows that

$$\mathbf{E}_{S(t)}[\bar{w}(t)] = \bar{v}(t). \tag{33}$$

Proof. First, we present a key observation given by ref. [35] as an important trick to handle the randomness caused by client selection with probability distribution $\{q_k\}_{k=1}^N$. By taking the expectation over S(t), it follows that

$$E_{S(t)} \sum_{k \in S(t)} X_k = K E_{S(t)}[X_k] = K \sum_{k=1}^N q_k X_k.$$
 (34)

Let $q_k = \rho_k$, take the expectation of $\bar{w}(t)$ over S(t) and notice that $\bar{v}(t) = \sum_{k \in U} \rho_k v_k(t)$:

$$\mathbf{E}_{S(t)}[\bar{w}(t)] = \mathbf{E}_{S(t)} \left[\frac{1}{K} \sum_{k \in S(t)} v_k(t) \right]$$

$$= \frac{1}{K} \mathbf{E}_{S(t)} \right] \sum_{k \in S(t)} [v_k(t)]$$

$$= \frac{1}{K} K \mathbf{E}_{S(t)} [v_k(t)]$$

$$= \sum_{k \in U} q_k v_k(t)$$

$$= \bar{v}(t).$$

Lemma 5 (Bounded variance of $\bar{w}(t)$). For any aggregation step $t \in T_A$ and with a non-increasing step size η_t s.t. $\eta_t \leq 2\eta_{t+E-1}$, it follows that

$$\mathbf{E}_{S(t)} \|\bar{w}(t) - \bar{v}(t)\|^2 \le \frac{4}{K} \eta_{t-1}^2 E^2 G^2. \tag{35}$$

Proof. First, one can prove that $v_k(t)$ is an unbiased estimate of $\bar{v}(t)$ for any k:

$$E_{S(t)}[v_k(t)] = \sum_{k \in II} q_k v_k(t) = \bar{v}(t).$$
(36)

Then by the aggregation rule $\bar{w}(t) = \frac{1}{K} \sum_{k \in S(t)} v_k(t)$, we have:

$$E_{S(t)} \|\bar{w}(t) - \bar{v}(t)\|^{2} = \frac{1}{K^{2}} E_{S(t)} \|K\bar{w}(t) - K\bar{v}(t)\|^{2}
= \frac{1}{K^{2}} E_{S(t)} \|\sum_{k \in S(t)} v_{k}(t) - \sum_{k=1}^{K} \bar{v}(t)\|^{2}
= \frac{1}{K^{2}} E_{S(t)} \|\sum_{k \in S(t)} \left(v_{k}(t) - \bar{v}(t)\right)\|^{2}
= \frac{1}{K^{2}} \left(E_{S(t)} \sum_{k \in S(t)} \|v_{k}(t) - \bar{v}(t)\|^{2}
+ E_{S(t)} \sum_{i,j \in S(t), i \neq j} \langle v_{i}(t) - \bar{v}(t), v_{j}(t) - \bar{v}(t) \rangle\right), \tag{37}$$

where the second term on the RHS of (37) equals zero because $\{v_k(t)\}_{k\in U}$ are independent and unbiased (see Eq. 36). Further, by noticing $t-E\in T_A$ (because $t\in T_A$) which implies that $w_k(t-E)=\bar{w}(t-E)$ since the last communication, we have:

$$E_{S(t)} \|\bar{w}(t) - \bar{v}(t)\|^{2} = \frac{1}{K^{2}} E_{S(t)} \sum_{k \in S(t)} \|v_{k}(t) - \bar{v}(t)\|^{2}
= \frac{1}{K^{2}} K E_{S(t)} \|v_{k}(t) - \bar{v}(t)\|^{2}
= \frac{1}{K} E_{S(t)} \|(v_{k}(t) - \bar{w}(t-E)) - (\bar{v}(t) - \bar{w}(t-E))\|^{2}
\leq \frac{1}{K} E_{S(t)} \|v_{k}(t) - \bar{w}(t-E)\|^{2},$$
(38)

where the last inequality results from $\mathrm{E}[v_k(t)-\bar{w}(t-E)]=\bar{v}(t)-\bar{w}(t-E)$ and that $\mathrm{E}\|X-\mathrm{E}X\|^2\leq E\|X\|^2$. Further, we have:

$$E_{S(t)} \|\bar{w}(t) - \bar{v}(t)\|^{2} \leq \frac{1}{K} E_{S(t)} \|v_{k}(t) - \bar{w}(t - E)\|^{2}
= \frac{1}{K} \sum_{k=1}^{N} q_{k} E_{S(t)} \|v_{k}(t) - \bar{w}(t - E)\|^{2}
= \frac{1}{K} \sum_{k=1}^{N} q_{k} \underbrace{E_{S(t)}}_{i=t-E} \|\sum_{k=1}^{t-1} \eta_{i} \nabla F_{k}(w_{k}(i), \xi_{k,i})\|^{2} .$$
(39)

Let $i_m = \arg\max_i \|\nabla F_k(w_k(i), \xi_{k,i})\|, i \in [t-E, t-1]$. By using the Cauchy-Schwarz inequality, Assumption 4 and choosing a non-increasing η_t s.t. $\eta_t \leq 2\eta_{t+E-1}$, we have:

$$Z_{1} = \mathbf{E}_{S(t)} \| \sum_{i=t-E}^{t-1} \eta_{i} \nabla F_{k}(w_{k}(i), \xi_{k,i}) \|^{2}$$

$$= \sum_{i=t-E}^{t-1} \sum_{j=t-E}^{t-1} \mathbf{E}_{S(t)} \langle \eta_{i} \nabla F_{k}(w_{k}(i), \xi_{k,i}), \eta_{j} \nabla F_{k}(w_{k}(j), \xi_{k,j}) \rangle$$

$$\leq \sum_{i=t-E}^{t-1} \sum_{j=t-E}^{t-1} \mathbf{E}_{S(t)} \Big[\| \eta_{i} \nabla F_{k}(w_{k}(i), \xi_{k,i}) \| \cdot \| \eta_{j} \nabla F_{k}(w_{k}(j), \xi_{k,j}) \| \Big]$$

$$\leq \sum_{i=t-E}^{t-1} \sum_{j=t-E}^{t-1} \eta_{i} \eta_{j} \cdot \mathbf{E}_{S(t)} \| \nabla F_{k}(w_{k}(i_{m}), \xi_{k,i_{m}}) \|^{2}$$

$$\leq \sum_{i=t-E}^{t-1} \sum_{j=t-E}^{t-1} \eta_{t-E}^{2} \cdot \mathbf{E}_{S(t)} \| \nabla F_{k}(w_{k}(i_{m}), \xi_{k,i_{m}}) \|^{2}$$

$$\leq 4 \eta_{t-1}^{2} E^{2} G^{2}. \tag{40}$$

Plug Z_1 back into (39) and notice that $\sum_{k=1}^{N} q_k = 1$, we have:

$$\begin{aligned} \mathbf{E}_{S(t)} \|\bar{w}(t) - \bar{v}(t)\|^2 &\leq \frac{1}{K} \sum_{k=1}^{N} q_k 4\eta_t^2 E^2 G^2 \\ &= \frac{4}{K} \eta_{t-1}^2 E^2 G^2. \end{aligned}$$

D. Proof of Theorem 1

Proof. Taking expectation of $\|\bar{w}(t) - w^*\|^2$ over S(t), we have:

$$\mathbf{E}_{S(t)} \|\bar{w}(t) - w^*\|^2 = \mathbf{E}_{S(t)} \|\bar{w}(t) - \bar{v}(t) + \bar{v}(t) - w^*\|^2 \\
= \underbrace{\mathbf{E}_{S(t)} \|\bar{w}(t) - \bar{v}(t)\|^2}_{A_1} + \underbrace{\mathbf{E} \|\bar{v}(t) - w^*\|^2}_{A_2} + \underbrace{\mathbf{E}_{S(t)} \langle \bar{w}(t) - \bar{v}(t), \bar{v}(t) - w^* \rangle}_{A_2} \tag{41}$$

where A_3 vanishes because $\bar{w}(t)$ is an unbiased estimate of $\bar{v}(t)$ (Lemma 4) and A_2 is independent of S(t). To bound A_2 for $t \in T_A$, we apply Lemma 1:

$$A_{2} = \mathbb{E}\|\bar{v}(t) - w^{*}\|^{2} \leq (1 - \eta_{t-1}\mu)\mathbb{E}\|\bar{w}(t-1) - w^{*}\|^{2} + \underbrace{\eta_{t-1}^{2}\mathbb{E}\|g_{t-1} - \bar{g}_{t-1}\|^{2}}_{B_{1}} + 6L\eta_{t-1}^{2}\Gamma + \underbrace{\mathbb{E}\left[\sum_{k=1}^{N}\rho_{k}\|w_{k}(t-1) - \bar{w}(t-1)\|^{2}\right]}_{B_{2}}.$$

$$(42)$$

Then we use Lemmas 2 and 3 to bound B_1 and B_2 respectively, which yields:

$$A_2 = \mathbb{E}\|\bar{v}(t) - w^*\|^2 \le (1 - \eta_{t-1}\mu)\mathbb{E}\|\bar{w}(t-1) - w^*\|^2 + \eta_{t-1}^2\mathcal{B},\tag{43}$$

where $\mathcal{B}=\sum_{k=1}^N \rho_k^2 \epsilon_k^2 + 6L\Gamma + 8(E-1)^2 G^2.$ Then we bound A_1 with Lemma 5:

$$A_1 = \mathcal{E}_{S(t)} \|\bar{w}(t) - \bar{v}(t)\|^2 \le \frac{4}{K} \eta_{t-1}^2 E^2 G^2$$
(44)

Let $C = \frac{4}{K}E^2G^2$ and plug A_1 and A_2 back into (41):

$$E_{S(t)}\|\bar{w}(t) - w^*\|^2 \le (1 - \eta_{t-1}\mu)E_{S(t)}\|\bar{w}(t-1) - w^*\|^2 + \eta_{t-1}^2(\mathcal{B} + \mathcal{C}). \tag{45}$$

Equivalently, let $\Delta_t = \mathrm{E}_{S(t)} \|\bar{w}(t) - w^*\|^2$, then we have the following recurrence relation for any $t \geq 1$:

$$\Delta_t \le (1 - \eta_{t-1}\mu)\Delta_{t-1} + \eta_{t-1}^2(\mathcal{B} + \mathcal{C}). \tag{46}$$

Next we prove by induction that $\Delta_t \leq \frac{\nu}{\gamma + t}$ where $\nu = \max\left\{\frac{\beta^2(\mathcal{B} + \mathcal{C})}{\beta \mu - 1}, (\gamma + 1)\Delta_1\right\}$ using an aggregation interval $E \geq 1$ and a diminishing step size $\eta_t = \frac{\beta}{t + \gamma}$ for some $\beta > \frac{1}{\mu}$ and $\gamma > 0$ such that $\eta_1 \leq \min\{\frac{1}{\mu}, \frac{1}{4L}\}$ and $\eta_t \leq 2\eta_{t+E}$.

First, for t=1 the conclusion holds that $\Delta_1 \leq \frac{\nu}{\gamma+1}$ given the conditions. Then by assuming it holds for some t, one can derive from (46) that

$$\Delta_{t+1} \leq (1 - \eta_t \mu) \Delta_t + \eta_t^2 (\mathcal{B} + \mathcal{C})
\leq \left(1 - \frac{\beta \mu}{t + \gamma}\right) \frac{\nu}{\gamma + t} + \left(\frac{\beta}{t + \gamma}\right)^2 (\mathcal{B} + \mathcal{C})
= \frac{t + \gamma - 1}{(t + \gamma)^2} \nu + \underbrace{\left[\frac{\beta^2 (\mathcal{B} + \mathcal{C})}{(t + \gamma)^2} - \frac{\beta \mu - 1}{(t + \gamma)^2} \nu\right]}_{\geq 0}
\leq \frac{t + \gamma - 1}{(t + \gamma)^2} \nu
\leq \frac{t + \gamma - 1}{(t + \gamma)^2 - 1} \nu
= \frac{\nu}{t + \gamma + 1},$$
(47)

which proves the conclusion $\Delta_t \leq \frac{\nu}{\gamma + t}$ for any $t \geq 1$.

Then by the smoothness of the objective function F, it follows that

$$E_{S(t)}[F(\bar{w}(t))] - F^* \le \frac{L}{2} E_{S(t)} \|\bar{w}(t) - w^*\|^2
= \frac{L}{2} \Delta_t \le \frac{L}{2} \frac{\nu}{\gamma + t}.$$
(48)

Specifically, by choosing $\beta=\frac{2}{\mu}$ (i.e., $\eta_t=\frac{2}{\mu(\gamma+t)}$), $\gamma=\max\{\frac{8L}{\mu},E\}-1$, we have

$$\nu = \max \left\{ \frac{\beta^2 (\mathcal{B} + \mathcal{C})}{\beta \mu - 1}, (\gamma + 1) \Delta_1 \right\}$$

$$\leq \frac{\beta^2 (\mathcal{B} + \mathcal{C})}{\beta \mu - 1} + (\gamma + 1) \Delta_1$$

$$= \frac{4(\mathcal{B} + \mathcal{C})}{\mu^2} + (\gamma + 1) \Delta_1.$$
(49)

By definition, we have $w(t) = \bar{w}(t)$ at the aggregation steps. Therefore, for $t \in T_A$:

$$E_{S(t)}[F(w(t))] - F^* \le \frac{L}{2} \frac{\nu}{\gamma + t}$$

$$= \frac{L}{(\gamma + t)} \left(\frac{2(\mathcal{B} + \mathcal{C})}{\mu^2} + \frac{\gamma + 1}{2} \Delta_1 \right).$$

APPENDIX D

PROFILE DISSIMILARITY UNDER HOMOMORPHIC ENCRYPTION

The proposed representation profiling scheme encodes the representations of data into a list of distribution parameters, namely $RP(\boldsymbol{w},D) = \{(\mu_i,\sigma_i^2)|i=1,2,\ldots,q\}$ where q is the length of the profile. Theoretically, the information leakage (in terms of the data in D) by exposing $RP(\boldsymbol{w},D)$ is very limited and it is basically impossible to reconstruct the samples in D given $RP(\boldsymbol{w},D)$. Nonetheless, Homomorphic Encryption (HE) can be applied to the profiles (both locally and on the server) so as to guarantee zero knowledge disclosure while still allowing profile matching under the encryption. In the following we give details on how to encrypt a representation profile and compute profile dissimilarity (with decryption) using Homomorphic Encryption (HE).

To calculate (3) and (4) under encryption, a client needs to encrypt (denoted as $[[\cdot]]$) every single μ_i and σ_i^2 in its profile $RP(\boldsymbol{w},D)$ locally before upload whereas the server does the same for its $RP^*(\boldsymbol{w},D^*)$. Therefore, according to Eq. (4) we have:

$$[[KL(\mathcal{N}_{i}^{(k)}||\mathcal{N}_{i}^{*})]] = \frac{1}{2}\log[[(\sigma_{i}^{*})^{2}]] - \frac{1}{2}\log[[(\sigma_{i}^{(k)})^{2}]] - [[\frac{1}{2}]] + \frac{([[(\sigma_{i}^{(k)})^{2}]] + ([[\mu_{i}^{(k)}]] - [[\mu_{i}^{*}]])^{2}}{2[[(\sigma_{i}^{*})^{2}]]},$$
(50)

where the first two terms on the right-hand side require logarithm operation on the ciphertext. However, this may not be very practical because most HE schemes are designed for basic arithmetic operations on the ciphertext. Thus we also consider the situation where HE scheme at hand only provides additive and multiplicative homomorphisms [56]. In this case, to avoid the logarithm operation, the client needs to keep every σ_i^2 in $RP^*(\boldsymbol{w}, D_i)$ as plaintext and only encrypts μ_i , likewise for the server. As a result, the KL divergence can be computed under encryption as:

$$[[KL(\mathcal{N}_{i}^{(k)}||\mathcal{N}_{i}^{*})]] = \left[\left[\frac{1}{2} \log(\frac{\sigma_{i}^{*}}{\sigma_{i}^{(k)}})^{2} + \frac{1}{2} \left(\frac{\sigma_{i}^{(k)}}{\sigma_{i}^{*}}\right)^{2} - \frac{1}{2} \right] \right] + \frac{1}{2(\sigma_{i}^{*})^{2}} ([[\mu_{i}^{(k)}]] - [[\mu_{i}^{*}]])^{2}$$
(51)

where the first term on the right-hand side is encrypted after calculation with plaintext values $(\sigma_i^k)^2$ and $(\sigma^*)^2$ whereas the second term requires multiple operations on the ciphertext values $[[\mu_i^k]]$ and $[[\mu^*]]$. Now, in either case, we can compute profile dissimilarity under encryption according to Eq. (52):

$$[[div(RP_k, RP^*)]] = \frac{1}{q} \sum_{i=1}^{q} [[KL(\mathcal{N}_i^{(k)}||\mathcal{N}_i^*)]]$$
(52)

APPENDIX E DETAILS OF EXPERIMENTAL SETUP

A. Environment Setup

TABLE IV: Experimental setup.

Setting	Symbol	S-Task	L-Task
Model	\overline{w}	FFN	CNN
Dataset	D	GasTurbine	EMNIST digits
Total data size	D	36.7k	280k
Validation (benchmark) set size	$ D^* $	11.0k	40k
Client population	n	50	1000
Data distribution	-	$\mathcal{N}(514, 154^2)$	non-IID, dominant≈60%
Noise applied	-	fake, gaussian noise	fake, blur, s&p
Client specification (GHz)	s_k	$\mathcal{N}(0.5, 0.1^2)$	$\mathcal{N}(1.0, 0.1^2)$
Comm. bandwidth (MHz)	bw_k	$\mathcal{N}(0.5, 0.1^2)$	$\mathcal{N}(1.0, 0.1^2)$
Signal-noise ratio	SNR	1e2	1e2
Bits per sample	BPS	11*8*8	28*28*1*8
Cycles per bit	CPB	300	400
# of local epochs	E	2	5
Loss function	ℓ	MSE Loss	NLL Loss
Learning rate	η	1e-2	1e-2
learning rate decay	-	0.99	0.99

Detailed experimental settings are listed in Table IV. In the S-Task, the total population is 50 and the data collected by a proportion of the sensors (i.e., end devices of this task) are of low-quality: 10% of the sensors have no valid data and 40% of them produce noisy data. In the L-Task, we set up a relatively large population (1000 end devices) and spread the data (from *EMNIST digits*) across the devices with strong class imbalance – roughly 60% of the samples on each device fall into the same class. Besides, many local datasets are of low-quality: the images on 15% of the clients are irrelevant (valueless for the training of this task), 20% are (Gaussian) blurred, and 25% are affected by the salt-and-pepper noise (random black and white dots on the image, density=0.3). For the S-Task, the maximum number of rounds t_{max} is set to 100 for both aggregation modes, whilst it is set to 300 and 50 for the full aggregation and partial aggregation, respectively, for the L-Task. The preference factor α for our protocol is set to 10. Considering the population of the clients, the setting of the selection fraction C is based on the scale of the training participants suggested in ref. [5].

To simulate a realistic FL system that consists of disparate end devices, the clients are heterogeneous in terms of both performance and communication bandwidth (see Table IV). A validation set is kept by the server (as the benchmark data) and used for model evaluation.

B. Details of Cost Formulation

In each FL round, the server selects a fraction (i.e., C) of clients, distributes the global model to these clients and waits for them to finish the local training and upload the models. Given a selected set of clients S(t), the time cost and energy cost of a communication round can be formulated as:

$$T_{round} = \max_{k \in S(t)} \{ T_k^{comm} + T_k^{train} + T_k^{RP} \}, \tag{53}$$

$$E_k = E_k^{comm} + E_k^{train} + E_k^{RP}. (54)$$

where T_k^{comm} and T_k^{train} are the communication time and local training time, respectively. The deviceside energy consumption E_k mainly comes from model transmission (through wireless channels) and local processing (training), corresponding to E_k^{comm} and E_k^{train} , respectively. T_k^{RP} and E_k^{RP} estimate the time and energy costs for generating and uploading local profiles and only apply to FEDPROF.

Eq. (53) formulates the length of one communication round of FL, where T_k^{comm} can be modeled by Eq. (55) according to ref. [52], where bw_k is the downlink bandwidth of device k (in MHz); SNR is the Signal-to-Noise Ratio of the communication channel, which is set to be constant as in general the end devices are coordinated by the base stations for balanced SNR with the fairness-based policies; msize is the size of the model; the model upload time is twice as much as that for model download since the uplink bandwidth is set as 50% of the downlink bandwidth.

$$T_k^{comm} = T_k^{upload} + T_k^{download}$$

$$= 2 \times T_k^{download} + T_k^{download}$$

$$= 3 \times \frac{msize}{bw_k \cdot \log(1 + SNR)},$$
(55)

 T_k^{train} in Eq. (53) can be modeled by Eq. (56), where s_k is the device performance (in GHz) and the amount of work in local training; the numerator computes the total number of processor cycles required for processing E epochs of local training on D_k .

$$T_k^{train} = \frac{E \cdot |D_k| \cdot BPS \cdot CPB}{s_k},\tag{56}$$

 T_k^{RP} consists of two parts: T_k^{RPgen} for local model evaluation (to generate the profiles of D_k) and T_k^{RPup} for uploading the profile. T_k^{RP} can be modeled as:

$$\begin{split} T_k^{RP} &= T_k^{RPgen} + T_k^{RPup} \\ &= \frac{1}{E} T_k^{train} + \frac{RPsize}{\frac{1}{2} b w_k \cdot \log(1 + SNR)}, \end{split} \tag{57}$$

where T_k^{RPgen} is estimated as the time cost of one epoch of local training; T_k^{RPup} is computed in the the similar way as calculating T_k^{comm} in Eq. (55) (the uplink bandwidth is set as one half of the total bw_k); RPsize is the size of a profile, which equals to $4 \times 2 \times q = 8 \times q$ (four bytes for each floating point number) according to our definition of profile in Eq. (2).

Using Eq. (54) we model the energy cost of each end device by mainly considering the energy consumption of the transmitters for communication (Eq. 58) and on-device computation for local training (Eq. 59). In our protocol, there is an extra energy cost for generating and uploading profiles (Eq. 60).

$$E_k^{comm} = P_{trans} \cdot T_k^{comm} \tag{58}$$

$$E_k^{train} = P_f s_k^3 \cdot T_k^{train} \tag{59}$$

$$E_k^{RP} = P_{trans} \cdot T_k^{RPup} + P_f s_k^3 \cdot T_k^{RPgen}, \tag{60}$$

where $P_f s_k^3$ is a simplified computation power consumption model [57] and P_f is the power of a baseline processor. P_{trans} is the transmitter's power. We set P_{trans} and P_f to 0.5 and 0.7 Watts based on the benchmarking data provided by ref. [58].